Journal of Magnetism and Magnetic Materials 595 (2024) 171831

Contents lists available at ScienceDirect

Journal of Magnetism and Magnetic Materials

journal homepage: www.elsevier.com/locate/jmmm

Research article

Correlation between structural and improved magneto-dielectric behaviour of Li-Mg-Dy ferrite/Graphene nanoplatelet composites and their potential applications

Maria Akhtar [a], Atta Ur Rehman [a], Nasir Amin [a], Khalid Hussain [a], Muhammad Imran Arshad [a,b,c,*]

[a] Department of Physics, Government College University, Faisalabad, Pakistan
[b] Biophysics Group, Department of Physics and Astronomy, University College London, Gower Street, London WC1E 6BT, UK
[c] UCL Healthcare Biomagnetics and Nanomaterials Laboratories, 21 Albemarle Street, London W1S 4BS, UK

ARTICLE INFO

Keywords:
Graphene nanoplatelets
Spinel
Composites
Raman
Magneto-dielectric

ABSTRACT

The tenacity of the current study was to prepare $Li_{0.2}Mg_{0.6}Fe_{2.17}Dy_{0.03}O_4$/Graphene nanoplatelet (***LMFD/GNP***) composites with different Graphene nanoplatelets (GNPs) contents, including 0 wt% GNPs, 1.25 wt% GNPs, 2.5 wt% GNPs, 3.75 wt% GNPs, and 5 wt% GNPs using an economical chemical sol–gel auto combustion (SGAC) process, with a balance among the structural, and magneto-dielectric order parameters for potential applications. The structural study indicated all the LMFD/GNP composites have single-phase spinel matrix and maximum crystallite size was 53.32 nm, while Lorentz fit Raman spectra also confirmed the spinel matrix along with the existence of GNPs in the composites. The LMFD/GNP composites revealed a decrease in dielectric constants and tangent loss with increasing frequency and higher values at low frequencies, while lower values at high frequencies. The quality factor was maximum and tangent loss was the minimum for LMFD/GNP composite with GNPs doping 1.25 wt% GNPs. The LMFD/GNP composites were found to have a soft magnetic nature and the composite with GNPs concentration of 2.5 wt% GNPs has the highest saturation magnetization (104.59 emu/g) and microwave operating frequency (23.12 GHz). Moreover, the retentivity and high coercivity were 32.85 emu/g and 107.99 Oe for 1.25 wt% GNPs composite. Due to a comparatively high crystallite size, large saturation magnetization, and microwave operating frequency along with high coercivity the LMFD/GNP composites are well suited for potential applications including high-frequency devices, transformer cores, and hyperthermia.

1. Introduction

Multifunctional composites made of magnetic materials and graphene nanoplatelets (GNPs) have recently attracted a lot of interest. Large surface areas of GNPs, a wonder material with exceptional mechanical, electrical, and thermal properties, can be employed as a template for the improvement of the properties of magnetic materials [1–6] and useful for the production of composites [7]. High specific surface area and low aggregation GNP-based materials have strong organic pollutant adsorption capabilities. As a result, it's essential to avoid aggregation between the layers. Magnetic graphene composites are made by adding magnetic particles to the adsorbent for easy separation [8]. Graphene-based composites have various uses across many industries, including optoelectronics, photoelectrochemistry, photo-catalysis, bio-imaging, electrochemical sensors, and photovoltaics [9,10], as well as suitable for controlled damping, vibrational absorption, or automotive bushings [11], stretchable magnetic materials [12], and soft applications, such as flexible electronics [13].

The extraordinary properties of spinel ferrites (SFs) including their chemical, physical, and electrical properties make these substances one of the greatest subjects of interest for researchers in the fields of nanoscience, nanoelectronics, and nanotechnology [14–17]. The SFs are chemically expressed as MFe_2O_4 where M is a divalent metal cation. The high electrical resistivity of these materials makes them particularly useful in high-frequency applications, as they minimize eddy current losses in alternating current fields. Gas sensors [18], and microwave communication systems [19] are some common applications of SFs. The SF's dielectric, magnetic, physical, and electrical properties were

* Corresponding author at: Department of Physics, Government College University, Faisalabad, Pakistan.
E-mail addresses: muhammad.arshad@ucl.edu.pk, mimranarshad@gcuf.edu.pk, miarshad15@gmail.com (M. Imran Arshad).

https://doi.org/10.1016/j.jmmm.2024.171831
Received 22 April 2023; Received in revised form 30 January 2024; Accepted 3 February 2024
Available online 5 February 2024

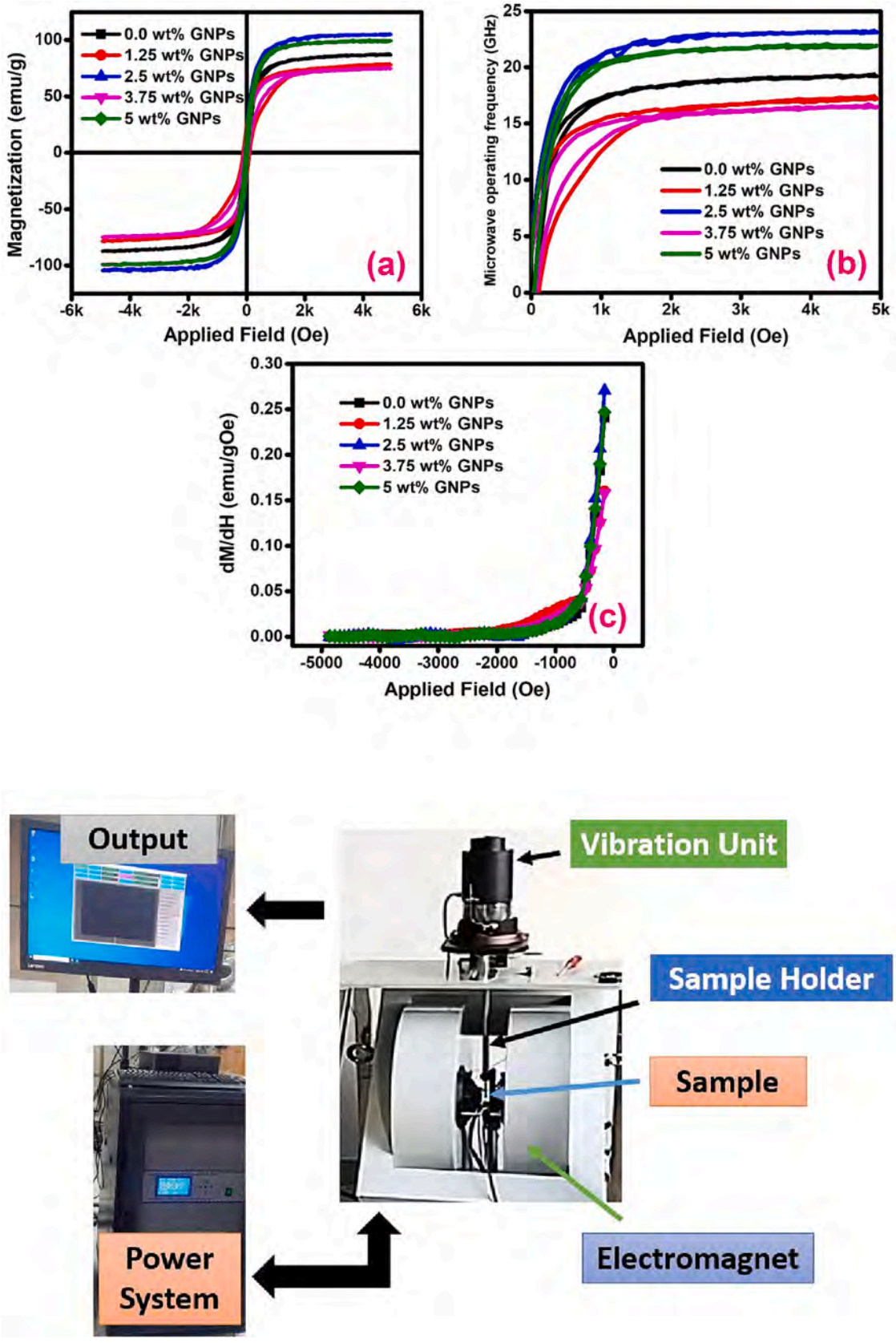

Fig. 1. VSM set-up and their assembly.

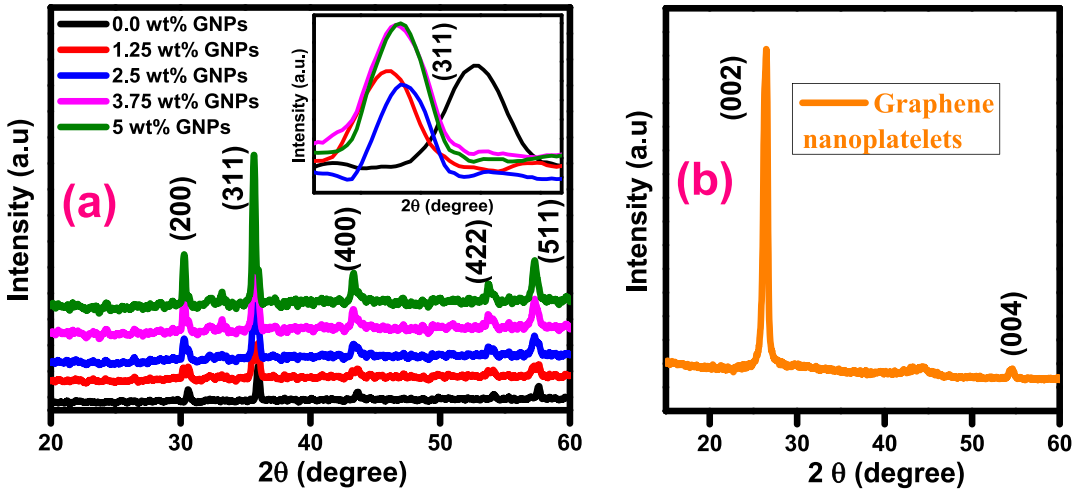

Fig. 2. (a) XRD pattern for LMFD/GNPs composites (b) XRD pattern for graphene nanoplatelets.

changed due to several factors including doping ions and changing concentration of dopant, the synthesis technique along with the conditions used during processing, and the type of cation used to replace Fe^{3+}/Fe^{2+} ions in the host crystal structure [20–23].

Few researchers, however, have used SFs combined with GNPs, which may have a special enhancement in the magneto-dielectric properties due to the combination of graphene's outstanding electrical conductivity and ferrite's amazing magnetic characteristics. The recently created innovative composites could be employed in high-frequency devices and are estimated to significantly improve the dielectric properties.

The hydrothermal process [24], mechanical milling method [25], co-precipitation technique [26], sol–gel auto combustion (SGAC) route [27–30], reverse microemulsion method [31], and radiofrequency plasma method [32] are the techniques used to synthesize composites. Among these methods, the SGAC method was used to prepare the composites due to: **(i)** The SGAC method typically results in highly homogeneous materials. It allows for precise control over the distribution of different elements and phases in the synthesized material. **(ii)** This method often produces fine particles and nano-scale particles, which can have unique properties and are useful in various applications, such as catalysis and nanomaterials. **(iii)** The SGAC process occurs at relatively low temperatures compared to other methods, reducing the energy input required for material synthesis. This is particularly advantageous for temperature-sensitive materials. **(iv)** The method allows for precise control over the stoichiometry of the final product, ensuring that the desired chemical composition is achieved. SGAC can be used to synthesize a wide range of materials, including oxides, ceramics, and composites. It can be adapted to produce materials with specific properties, such as magnetic, optical, or electrical properties. **(v)** The method allows for a choice of precursors, which can influence the final properties of the material. This flexibility can be used to tailor the material for specific applications. **(vi)** The method is considered environmentally friendly as it typically generates less waste and uses fewer hazardous reagents compared to other synthesis methods.

In this work, the SGAC method was used to prepare $Li_{0.2}Mg_{0.6}Fe_{2.17}Dy_{0.03}O_4$/Graphene nanoplatelet **[LMFD/GNP]** composites by varying GNPs concentration including 0 wt% GNPs, 1.25 wt% GNPs, 2.5 wt% GNPs, 3.75 wt% GNPs, and 5 wt% GNPs and studied the structural, and magneto-dielectric behaviour of the LMFD/GNP composites. The selection of GNPs, in particular, has gained significance as they exhibit exceptional structural, dielectric, and magnetic properties. Additionally, GNPs offer a high surface area and can be readily dispersed within matrices, making them an attractive choice for improving the performance of composite materials. In the pursuit of developing multifunctional composites, the control over the content of magnetic fillers like spinel ferrites, e.g., $Li_{0.2}Mg_{0.6}Fe_{2.17}Dy_{0.03}O_4$, is essential. The precise composition and concentration of these magnetic fillers influence the composite's magnetic properties, thereby impacting its suitability for applications such as electromagnetic shielding, data storage devices, sensors, and microwave devices. This study aims to elucidate the influence of GNPs on the properties of a $Li_{0.2}Mg_{0.6}Fe_{2.17}Dy_{0.03}O_4$/GNPs composite, specifically focusing on the magnetic properties. By controlling the content of GNPs, we explore the correlation between the properties of the composite and its potential suitability for diverse applications. Furthermore, we aim to understand the effect of GNPs on magnetic properties, their dispersion within the ferrite matrix, and the subsequent impact on the composite's overall performance. Our findings hold promise in contributing to the development of multifunctional nanocomposites for various practical applications.

2. Experimental part

2.1. Materials and method of preparation of LMFD/GNP composites

The SGAC process was applied to prepare $Li_{0.2}Mg_{0.6}Fe_{2.17}Dy_{0.03}O_4$/Graphene nanoplatelets (LMFD-GNPs) composites with various GNPs concentrations, including 0 wt% GNPs, 1.25 wt% GNPs, 2.5 wt% GNPs, 3.75 wt% GNPs, and 5 wt% GNPs. Highly pure analytical reagent grade chemicals were used as preliminary ingredients including Graphene nanoplatelets (25 μm particle size and surface area 120–150 m^2/g), dysprosium [$Dy(NO_3)_3{\cdot}6H_2O$] nitrate hexahydrate (99.9 %), magnesium [$Mg(NO_3)_2{\cdot}6H_2O$] nitrate hexahydrate (99.99 %), lithium [$LiNO_3{\cdot}6H_2O$] nitrate hexahydrate (99.99 %), and Iron [$Fe(NO_3)_3{\cdot}9H_2O$] nitrate nonahydrate (99.95 %) and purchased from Sigma-Aldrich. The chemicals were mixed in deionized water in a 1:1.2 proportion with citric acid as a fuel. The solution was then subjected to bath sonication to form the mixed nitrates and GNPs solution. The mixed solution was placed on a magnetic stirrer (MSR). Moreover. the solution pH 7 was maintained with the addition of dropwise ammonia solution. The powders were obtained by heating the solution to 80 °C to form a gel on a magnetic stirrer, which was then dried by increasing the temperature of the "MSR" up to 300 °C. The gel in dry form was taken and crushed to get a fine powder which was then put inside a muffle furnace for the sintering process and subjected to a heat of 800 °C for 8 h.

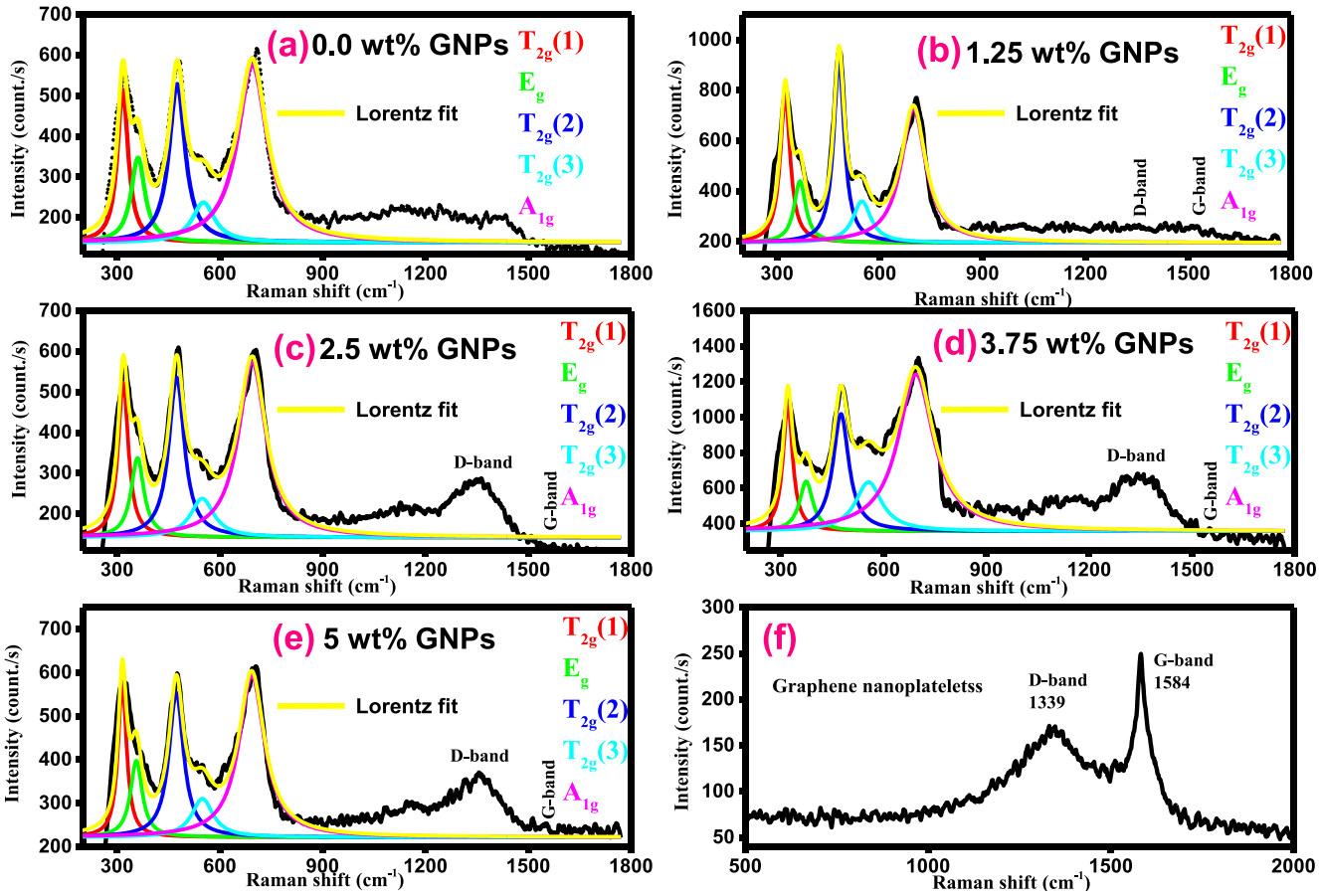

Fig. 3. (a) Raman spectra for the 0.0 wt%GNPs composite (b) Raman spectra for the 1.25 wt%GNPs composite (c) Raman spectra for the 1.25 wt%GNPs composite (c) Raman spectra for the 2.5 wt%GNPs composite (d) Raman spectra for the 3.75 wt%GNPs composite (e) Raman spectra for the 5 wt%GNPs composite (f) Raman spectra pure GNPs.

2.2. Characterizations used

With CuKα radiation (λ = 1.5406 Å) source, an X-ray diffractometer (PXRD, D8 ADVANCE, Bruker Corporation, Germany, 30 kV/35 mA) was employed for X-ray diffraction (XRD) investigation and the 50 mg sample was used for the measurements of data. The identification of vibrational modes was done through Raman spectroscopy (MNSTEX PRI 100, DongWoo Optron, South Korea) using a He-Ne laser source at 633.0 nm, while the LCR meter (Model IM3536, Japan, DC and 4 Hz to 8 MHz measurement frequency) helped to measure the dielectric properties. Vibrating-sample magnetometer (Model VSM-175, China) was used to measure the magnetic behaviour of LMFD/GNP composites. The VSM is a versatile method used to measure the magnetic moment of a sample as it undergoes perpendicular vibrations within a consistent magnetizing field. Each sample was taken in the powder form of 0.03 g and measured the magnetic moment in emu (electromagnetic unit) in the range of applied field ± 5kOe, then it was converted into magnetic moment per gram (emu/g). The VSM set-up with details and their assembly is shown in Fig. 1.

3. Results and discussion

3.1. Structural analysis of LMFD/GNP composites

Fig. 2(a) displayed the XRD spectra of LMFD/GNP composites. These patterns indicate that all the samples have (311), (220), (440), (400), and (511) planes, which confirms the spinel matrix was formed [33,34]. Fig. 2(b) illustrated the pure GNPs XRD pattern, while it was found that (002) and (004) peaks in pure GNPs. However, no peaks indicating the presence of GNPs were observed in all the as-prepared composites. Moreover, it was noticed that slight (311) peak shifts towards a smaller angle with the addition of GNPs, which confirmed the formation of LMFD/GNP composites. The peak with the highest intensity (311) of each sample was selected to determine the lattice constant (*a*), and crystallite size (*D*). The crystallite size was estimated *via* Scherrer's relation [35–38]. The crystallite size was 35.81 nm, 41.52 nm, 53.32 nm, 34.28 nm, and 32.11 nm for 0 wt% GNPs, 1.25 wt% GNPs, 2.5 wt% GNPs, 3.75 wt% GNPs, and 5 wt% GNPs composites. The addition of GNPs may introduce competing effects. For example, while some factors may promote the formation of smaller crystallites including enhanced nucleation sites, other factors may favour larger crystallite growth such as improved sintering efficiency. The balance between these factors can result in an irregular change in crystallite size. Also, the changes in GNP concentration can influence phase transitions within the material, leading to variations in crystallite size. Different phases may exhibit distinct crystallite growth behaviours. The effectiveness of GNPs as nucleation sites for crystallization may vary across the material. Regions with higher GNP concentrations may exhibit more effective nucleation and produce smaller crystallites, while other regions may not be as influenced. The distribution and dispersion of GNPs within the ferrite matrix can be non-uniform. Local variations in GNP distribution can lead to variations in crystallite size within the composite material [39,40]. Moreover, the lattice constant was 8.26 Å, 8.34 Å, 8.30 Å, 8.33 Å, and 8.34 Å for 0 wt% GNPs, 1.25 wt% GNPs, 2.5 wt% GNPs, 3.75 wt% GNPs, and 5 wt% GNPs composites. It was found that no significant change in lattice constant with the addition of GNPs. This may be ascribed to the considerable dispersion and incorporation of GNPs into the LMFD lattice.

Table 1
Raman modes for all the composite.

Samples	Raman shift (cm^{-1})						
	T_{2g} (1)	E_g	T_{2g} (2)	T_{2g} (3)	A_{1g}	**D band**	**G band**
	Tetrahedral (*A*) Site	Octahedral (*B*) site			Tetrahedral (*A*) Site		
0.0 wt%GNPs	317.08	361.43	475.60	552.28	695.16	–	–
1.25 wt%GNPs	324.05	366.99	481.05	547.89	698.26	1353.55	1575.11
2.5 wt%GNPs	318.29	359.90	474.14	548.88	694.62	1354.71	1577.58
3.75 wt%GNPs	320.87	374.38	475.83	556.44	694.69	1320.24	1565.23
5 wt%GNPs	315.74	356.60	473.12	549.38	693.33	1350.22	1578.63

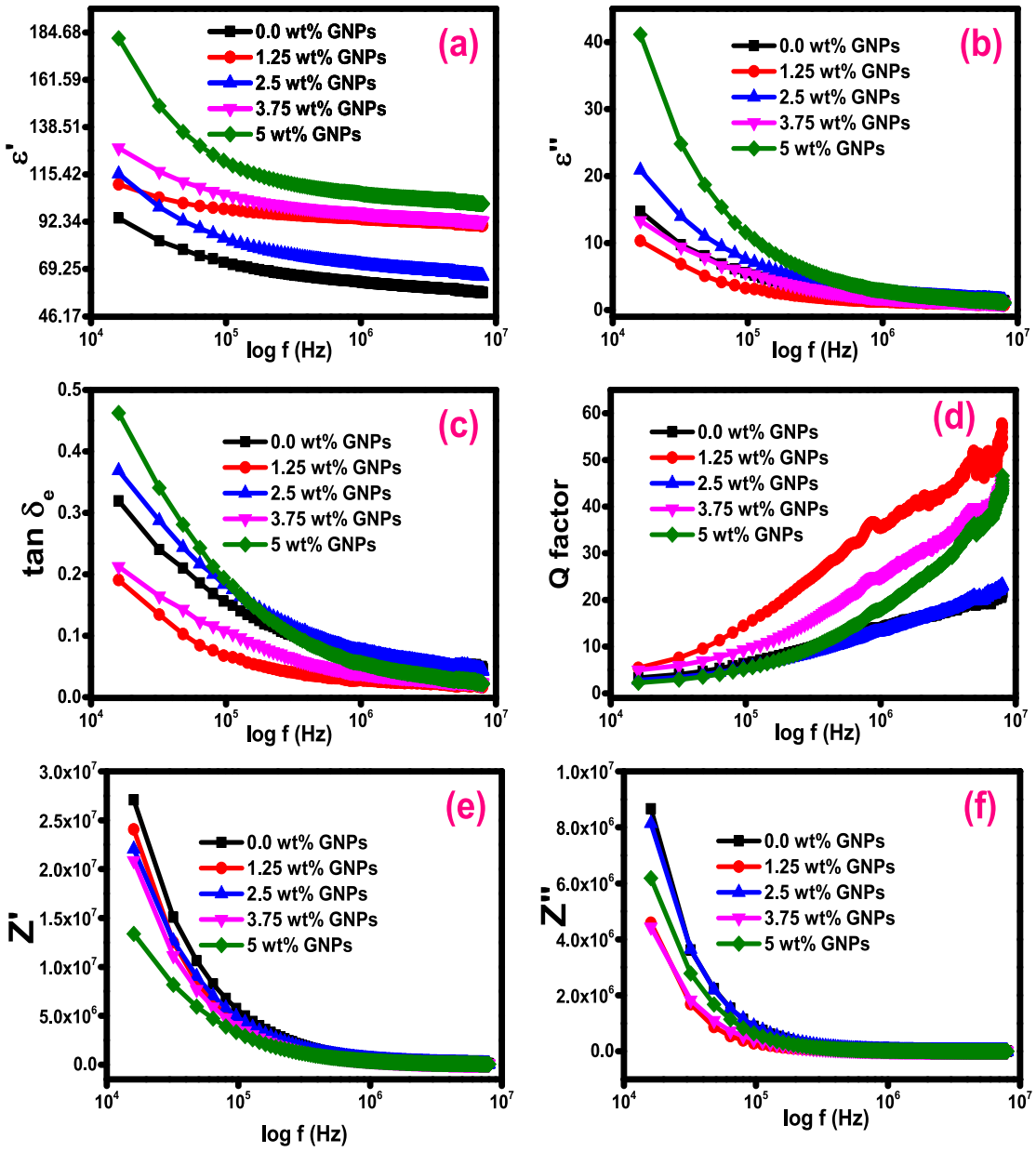

Fig. 4. (a) Frequency *versus* dielectric constant (real part) for LMFD/GNPs composite (b) Frequency *versus* dielectric loss (imaginary part) for LMFD/GNPs composite (c) Frequency *versus* tangent loss for LMFD/GNPs composite (d) Frequency *versus* quality factor for LMFD/GNPs composite (e) Frequency *versus* real part of impedance for LMFD/GNPs composite (e) Raman spectra for the 5 wt%GNPs composite (f) Frequency *versus* imaginary part of impedance for LMFD/GNPs composite.

3.2. Raman analysis of LMFD/GNP composites

The various Raman modes observed in SFs can be influenced by the chemical purity, synthesis technique, composition, and grain size of the sample. These modes are thought to be caused by the vibrations of different cations within the sample [41]. The existence of D-bands in the

Raman spectra for carbon-based material suggests the presence of defects in the carbon lattice. These defects may emerge during the preparation process and are commonly associated with sp^3 hybridized carbon atoms. The defect density in carbon-based materials is commonly determined by measuring the intensity of the D-band. Sp^2 hybridized carbon atoms are present in carbon-based materials due to the strong intensity of the G-band [42]. Lorentz fit Raman spectra having a range 250–1800 cm^{-1} for LMFD/GNP composites are displayed in Fig. 3(a–e), while Fig. 3(f) represented the pure GNPs spectra and exhibited that Raman bands around 1339 cm^{-1} attributed to D-band and, around 1584 cm^{-1} indicated the G-band. All the composites spectra showed the A_{1g} mode appeared in the range 693.33 cm^{-1}–698.26 cm^{-1}, which involves symmetrical vibrations of the oxygen atoms at *A*-site with respect to the metal ions, while T_{2g} (3) and *Eg* modes appeared around 549.38 cm^{-1}–556.44 cm^{-1} and 356.60 cm^{-1}–374.38 cm^{-1}, respectively, are caused by metal–oxygen and indicated symmetrical and asymmetrical vibration at *B*- site. The T_{2g} (2) mode, found at 473.12 cm^{-1}–481.05 cm^{-1} is caused by the asymmetric stretching at the *B* site, and the T_{2g} (1) mode present around 315.74 cm^{-1}–324.05 cm^{-1}, is caused by the translational motion of Fe-O_4 tetrahedron. The presence of these bands in the Raman spectra (as seen in Fig. 3) of all the composites suggested that LMFD/GNP contains all possible modes. The Raman band values are given in Table 1, although LMFD/GNP exhibited Raman peaks around 1320.24 cm^{-1}–1354.71 cm^{-1} and 1565.23 cm^{-1}–1578.63 cm^{-1} corresponds to the D band and G band of GNPs in addition to the presence of Raman active modes for the LMFD sample. The D band and G band peaks appeared to have low intensity at small concentration of GNPs, while intensity was increased with greater GNPs concentration. The variation in the D bands and G band along the peak shift was observed in XRD analysis both confirmed the existence of GNPs in the LMFD/GNP composites. Raman signatures also showed no secondary phase (also not seen in XRD spectra) was developed in LMFD/GNP composites due to the purity of the chemicals and synthesis method.

3.3. Dielectric properties

Dielectric measurement helps determine the dielectric parameters of the materials, particularly at high frequencies, which are necessary for many applications. These assessments provide valuable insights and are widely used in various industries including communication, material science, and microwave circuit design among others [43–45]. The log *f versus* real (ε') and imaginary (ε'') components of permittivity for LMFD/GNP composites at room temperature (*RT*) were plotted and displayed in Fig. 4(a) and Fig. 4(b), respectively. As frequency was increased, both ε' and ε'' were decreased, as depicted in Fig. 4(a) and Fig. 4(b), respectively. In all dielectric materials, it was found that both ε' and ε'' behave inversely with respect to frequency. According to Koop's theory, this is explained in terms of interfacial polarisation based on the Maxwell-Wagner type. There are oxygen vacancies in the material, which give rise to space charges when an external electric field (EEF) is applied, and are thought to be the cause of the free charges that form as a result of these defects. When the frequency is low, the charges have more time to travel farther into the material, producing a significant amount of electronic polarization and, consequently, a larger dielectric constant [46]. Fig. 4(c) illustrated frequency-dependant dielectric tangent loss (tan δ) plots. While more energy is needed for electron hopping between ferrous and ferric ions at low frequencies, it is clear that this causes higher dielectric at low frequencies. Due to the activation of highly conducting grains, which makes it easier for electrons to hop at low frequency, "tan δ" considerably drops as frequency rises, but further increases in frequency have little effect on the "tan δ" values. The "tan δ" had minimum value for composite graphene 1.25 wt% GNPs, as was seen in Fig. 4(c), and had a maximum value for 2.5 wt% GNPs composite at high frequency. The chemical composition, sintering temperature, crystallite size, frequency fluctuations, porosity, and reaction

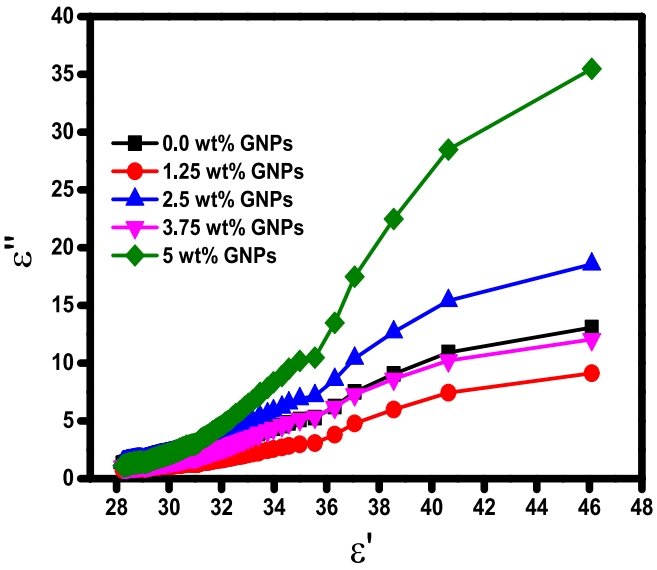

Fig. 5. Cole-Cole plots for LMFD/GNPs composites.

circumstances are only a few of the variables that affect the tangent loss [47,48]. The predictive capacity of the quality (*Q*) factor for diverse electrical devices and components arises from its ability to establish a link between the rate of energy dissipation and the stored energy, making it a valuable indicator of efficiency [49]. The quality (*Q*) factor is the reciprocal of the tangent loss [50] and the log *f versus Q* factor behaviour is illustrated in Fig. 4(d). It was noted that higher frequency ranges above 10^8 Hz have the highest value of *Q* factor and the composite with GNPs content 1.25 wt% GNPs had maximum value, while *Q* factor was minimum for a composite having GNPs concentration 2.5 wt % GNPs at high frequency. Hence, these composites can be used in resonance and high-frequency multilayer circuits.

Impedance investigation is the best method for assessing the bulk (grain) and grain-boundary contributions to the net conductivity and provides a comprehensive understanding of the electrical behaviour of SFs [50]. Fig. 4(e) and (f) showed all frequency-dependent real component of impedance (Z') and imaginary component (Z'') for all the compositions, respectively. As the frequency rises, the both Z' and Z'' was rapidly reduced. Moreover, with the addition of GNPs in LMFD sample, the both Z' and Z'' were reduced for all the composites. There is no

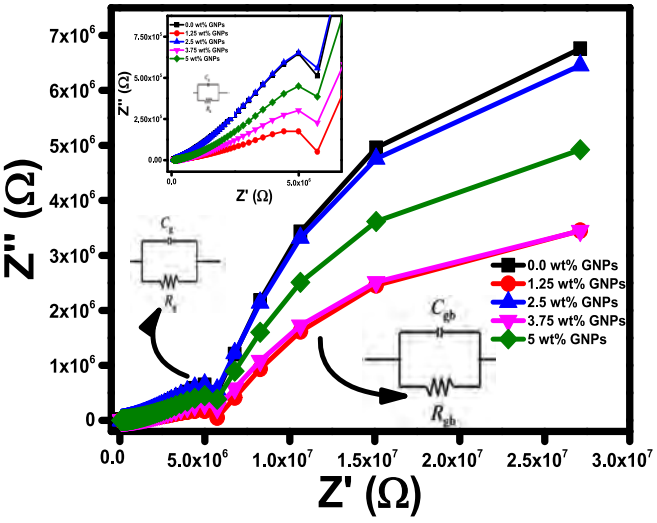

Fig. 6. Nyquist plots for LMFD/GNPs composites (with inside equivalent circuits).

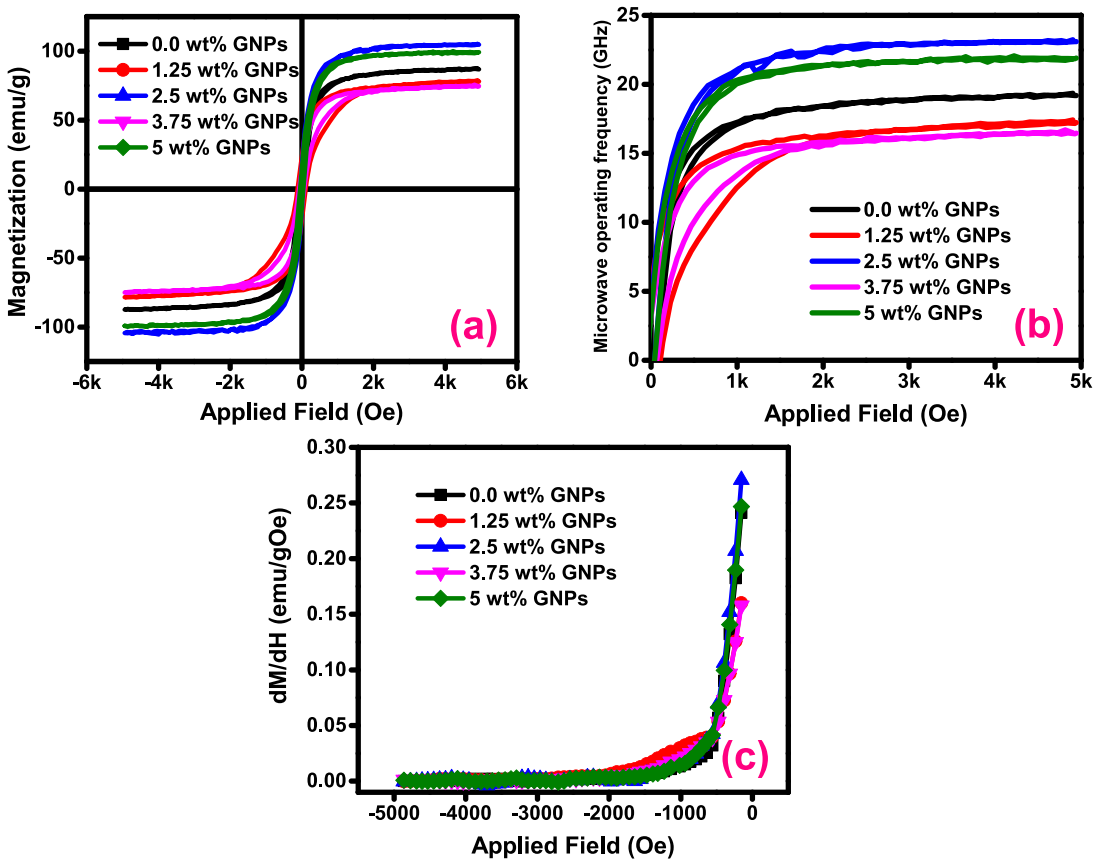

Fig. 7. (a) Applied field *versus* magnetization plots for LMFD/GNPs composites (b) Applied field *versus* microwave operating frequency plots for LMFD/GNPs composites (c) Applied field *versus* switching field distribution plots for LMFD/GNPs composites.

significant change in the impedance after around 10^6 Hz. A Cole-Cole plot is a valuable tool for characterizing the electrical behaviour of materials, particularly for dielectric properties. In this study, the Cole-Cole plot provides insights into the complex electrical response of the composite material. The deviations from a simple, idealized response can be indicative of various microstructural and electrical phenomena within the material [51]. Fig. 5 depicted Cole-Cole plots illustrating the variation of ε' and ε'' for LMFD/GNP composites. At low frequency, a linear behaviour is noticeable, and at high frequency, the linear response completely shifted to a semi-circle plot, indicating that the composites under investigation are insulating at low frequency and semi-conductive at high frequency. Grain boundaries seem to be electrically more resistive than the grains themselves due to their sound crystalline features. They are both thought to be two layers, with grain boundaries having large resistance and grains having small resistance. For instance, it may offer insights into the material's suitability for applications like sensors, where the dielectric properties are crucial. It can also inform the design of materials for electromagnetic interference (EMI) shielding or energy storage, where a tailored electrical response is vital [30]. Fig. 6 displayed the Nyquist plots of LMFD composites at room temperature in which the real (Z') and imaginary (Z'') components plotted along the *x*- and *y*-axes, respectively. On a Z' *versus* Z'' plots, a single semicircle at a high frequency indicates the existence of the grain impact, a second semicircle at a lower frequency shows the existence of the grain boundary influence, and a third semicircular arc is caused by the electrode effect [52]. All the LMFD/GNP composites exhibit two semicircular arcs, one at a higher frequency for the influence of the grain interior, and the other at a smaller frequency for the impact of the grain boundary. The random alignment of grains inside the two-dimensional conductivity gives rise to the grain boundary impedance. The parallel combination of grain boundary resistance and capacitance contributes

Table 2
Magnetic parameters of LMFD/GNPs composites.

Samples	H_C (Oe)	M_r (emu/g)	M_s (emu/g)	SQ	K (erg/cm^3)	ω_m (GHz)
0.0 wt% GNPs	65.07	40.10	86.86	0.4616	5887.47	19.20
1.25 wt% GNPs	107.99	32.85	78.01	0.4211	8775.31	17.24
2.5 wt% GNPs	43.18	30.65	104.59	0.2930	4704.37	23.12
3.75 wt% GNPs	67.17	21.94	74.52	0.2944	5214.07	16.47
5 wt% GNPs	41.77	29.47	99.15	0.2972	4314.05	21.92

to the impacts of the material's sample grain boundary. The discontinuities in Figs. 5 and 6 for spinel ferrites result from the presence of multiple relaxation processes in the material. Each discontinuity corresponds to a distinct relaxation phenomenon with its characteristic time constant, offering insights into the material's complex electrical and magnetic behaviour. These discontinuities can be attributed to the interplay of factors like microstructure, defect distribution, magnetic domains, and other material properties [53].

3.4. Magnetic properties

Fig. 7(a) illustrates the applied filed *versus* magnetization loops for LMFD/GNP composites. Table 2 exhibited the calculated magnetic parameters. The saturation magnetization (M_S) was maximum (104.59 emu/g) for 2.5 wt% GNPs composite. The maximum value of saturation

magnetization corresponds to the larger crystallite size of composite 2.5 wt% GNPs (as seen in XRD analysis). The enhancements in magnetic parameters with the addition of GNPs can be affected by different intrinsic and extrinsic parameters [8]. The relative distribution of cations at the *A*- and *B*- sites is one example of an intrinsic parameter. However, the *A*- and *B*- sites distribution of the cations is increased by the addition of GNPs in the LMFD lattice. Moreover, it alters the surface morphology and crystal strains. The extrinsic parameters are based on the density of the particles, morphology, and crystallite size. Further, Because of the addition of non-magnetic GNPs, the increase in M_S of the composite is probably caused by the effect of crystallite size and the number of magnetic particles present. In terms of crystallite size impact, a greater crystallite size tends to have larger M_S because of smaller magneto crystalline anisotropy and surface distortions of the particles [54]. The number of magnetic LMFD particles was fixed in the current study of LMFD/GNP composites, but the maximum saturation magnetization was observed for maximum crystallite size at 2.5 wt% GNPs. Table 2 shows that coercivity (H_C) was maximum (107.99 Oe) for composite has 1.25 wt% GNPs, while the value of 43.18 Oe for composite has 2.5 wt% GNPs. Moreover, the retentivity (M_r) decreased from 40.10 emu/g to 21.94 emu/g with an increase of GNPs from 0 wt% GNPs to 3.75 wt% GNPs and then increased up to 29.47 emu/g for 5 wt% GNPs composite. The anisotropy constant ($K = H_C \times M_S/0.96$) and squareness ratio ($SQ = M_r/M_S$) was calculated and reported in Table 2. The anisotropy constant showed anomalous behaviour and LMFD/GNP composites are single-domain nanoparticles with uniaxial anisotropy, as indicated by the SQ ratio being less than 0.5. The magnetic materials used for transformer cores and hyperthermia have minimal retentivity and coercivity [55]. The applied magnetic field *versus* microwave operating frequency ($\omega_m = 8\pi^2 M_s \gamma$ where gyromagnetic ratio = $\gamma = 2.8$ MHz/Oe) plots illustrated in Fig. 7(b). The maximum value of "ω_m" for composite having GNPs concentration 2.5 wt% GNPs composite is due to higher saturation magnetization. In Fig. 7(c), the *dM/dH versus* applied field (switching field distribution curves) was plotted and the *dM/dH* data showed a sharp increase in the small field (as displayed in Fig. 7(c)). It represents the distribution of magnetic switching fields within the material, reflecting the range of magnetic interactions and energies associated with the domains in the sample. The analysis of the switching field distribution (SDF) offers valuable insights into the domain behaviour and magnetic properties of the material. The SFD curves of the as-prepared composites are derived from the first derivative of the demagnetization data. Notably, the low-field switching response indicates weak magnetic interactions, while stronger magnetic interactions become evident at higher fields. The smooth and horizontal lines in the curves are indicative of strong magnetic interactions among the ions [56].

4. Conclusions

The technique of SGAC was employed to prepare LMFD/GNP composites having GNP concentrations 0 wt% GNPs, 1.25 wt% GNPs, 2.5 wt % GNPs, 3.75 wt% GNPs, and 5 wt% GNPs. XRD confirmed the creation of the spinel matrix attributed to single-phase. It was found that the "*D*" was maximum (53.32 nm) for 2.25 wt% GNPs composite. Lorentz fit Raman spectra also established the substitution of GNPs in the LMFD lattice. When the frequency was increasing, it was noted that there an exponential decay in the dielectric constant and tangent loss. The tangent loss and Q factor showed minimum and maximum values for composite have GNPs contents 1.25 wt% GNPs. Moreover, from VSM analysis the higher microwave operating frequency and saturation magnetization were observed for composite 2.5 wt% GNPs and the saturation magnetization has good agreement with crystallite size. Finally, it was concluded that based on the improved magneto-dielectric properties the LMFD/GNP composites are the best candidate for high-frequency application, transformer cores, and hyperthermia.

CRediT authorship contribution statement

Maria Akhtar: Writing – original draft. **Atta Ur Rehman:** Writing – review & editing. **Nasir Amin:** Validation. **Khalid Hussain:** Formal analysis. **Muhammad Imran Arshad:** Supervision, Conceptualization.

Declaration of competing interest

The authors declare that they have no known competing financial interests or personal relationships that could have appeared to influence the work reported in this paper.

Data availability

Data will be made available on request.

Acknowledgments

Muhammad Imran Arshad would like to thank HEC Pakistan for giving opportunity of Postdoc under post doc batch 3 (Ref: 3-1/PDFP/HEC/2022(B-3)/2320/02). He also extends his appreciation to University College London, London, U.K., for hosting this fellowship.

References

[1] F. Azizi, H. Jahangiri, Radar absorbing nanocomposites based multiLayered graphene platelets/epoxy, J. Nanostruct. 5 (2015) 345–349.
[2] A.U. Rehman, F. Afzal, M.T. Ansar, A. Sajjad, M.A. Munir, Introduction and Applications of 2D Nanomaterials, 2D Functional Nanomaterials: Synthesis, Characterization Applications (2021) 369–382.
[3] A. Maniadi, M. Vamvakaki, M. Suchea, I.V. Tudose, M. Popescu, C. Romanitan, C. Pachiu, O.N. Ionescu, Z. Viskadourakis, G. Kenanakis, Effect of graphene nanoplatelets on the structure, the morphology, and the dielectric behavior of low-density polyethylene nanocomposites, Materials 13 (2020) 4776.
[4] W. Chen, Q. Liu, X. Zhu, M. Fu, One-step in situ growth of magnesium ferrite nanorods on graphene and their microwave-absorbing properties, Appl. Organomet. Chem. 32 (2018) e4017.
[5] S. Deng, B. Wang, H. Ai, J. Han, Electromagnetic Wave Absorption Properties and Mechanism of Graphene/$Ni_{0.4}Zn_{0.6}Fe_2O_4$ Cement Composites, J. Mater. Civ. Eng. 34 (2022) 04022142.
[6] F.H. Mohammadabadi, S. Masoudpanah, S. Alamolhoda, H. Koohdar, Structure, magnetic, and microwave absorption properties of (MnNiCu) 0.9−xCoxZn0.1Fe2O4/graphene composite powders, J. Alloy. Compd. 878 (2021) 160337.
[7] V. Kumar, A. Kumar, M.N. Alam, S.S. Park, Effect of graphite nanoplatelets surface area on mechanical properties of room-temperature vulcanized silicone rubber nanocomposites, J. Appl. Polym. Sci. 139 (2022) e52503.
[8] E.E. Ateia, A.T. Mohamed, K. Elsayed, Impact of Gd3+/graphene substitution on the physical properties of magnesium ferrite nanocomposites, J. Magn. Magn. Mater. 452 (2018) 169–178.
[9] K. Takai, S. Tsujimura, F. Kang, M. Inagaki, Graphene: preparations, properties, applications, and prospects, (2019).
[10] N. Akhtar, M. Rani, A. Mahmood, K. Tariq, G. Murtaza, A.A. Alothman, R.S. AL-zahrani, S. Ali, N.K. Janjua, A. Shah, Synthesis and characterization of graphene oxide-based nanocomposite NaCr2O4/GO for electrochemical applications, J. Mater. Res. Technol. 15 (2021) 6287–6294.
[11] V. Kumar, D.-J. Lee, Iron particle and anisotropic effects on mechanical properties of magneto-sensitive elastomers, J. Magn. Magn. Mater. 441 (2017) 105–112.
[12] V. Kumar, M.N. Alam, S.-S. Park, D.-J. Lee, New insight into rubber composites based on graphene nanoplatelets, electrolyte iron particles, and their hybrid for stretchable magnetic materials, Polymers 14 (2022) 4826.
[13] V. Kumar, M.N. Alam, S.S. Park, Soft composites filled with iron oxide and graphite nanoplatelets under static and cyclic strain for different industrial applications, Polymers 14 (2022) 2393.
[14] S. Amiri, Shokrollahi, The role of cobalt ferrite magnetic nanoparticles in medical science, Mater. Sci. Eng. C 33 (2013) 1–8.
[15] X. Meng, H. Li, J. Chen, L. Mei, K. Wang, X. Li, Mössbauer study of cobalt ferrite nanocrystals substituted with rare-earth Y3+ ions, J. Magn. Magn. Mater. 321 (2009) 1155–1158.
[16] J.J. Vijaya, G. Sekaran, M. Bououdina, Effect of Cu2+ doping on structural, morphological, optical and magnetic properties of MnFe2O4 particles/sheets/flakes-like nanostructures, Ceram. Int. 41 (2015) 15–26.
[17] K. Manjunatha, I. Sathish, S. Kubrin, A. Kozakov, T. Lastovina, A. Nikolskii, K. Srinivasamurthy, M. Pasha, V.J. Angadi, X-ray photoelectron spectroscopy and low temperature Mössbauer study of Ce3+ substituted MnFe2O4, J. Mater. Sci. Mater. Electron. 30 (2019) 10162–10171.
[18] A. Sutka, G. Mezinskis, A. Lusis, M. Stingaciu, Gas sensing properties of Zn-doped p-type nickel ferrite, Sens. Actuators B 171 (2012) 354–360.

[19] V.G. Harris, A. Geiler, Y. Chen, S.D. Yoon, M. Wu, A. Yang, Z. Chen, P. He, P. V. Parimi, X. Zuo, Recent advances in processing and applications of microwave ferrites, J. Magn. Magn. Mater. 321 (2009) 2035–2047.

[20] X. Wu, Z. Ding, N. Song, L. Li, W. Wang, Effect of the rare-earth substitution on the structural, magnetic and adsorption properties in cobalt ferrite nanoparticles, Ceram. Int. 42 (2016) 4246–4255.

[21] A. Aslam, A.U. Rehman, N. Amin, M.A. un Nabi, Q. ul ain Abdullah, N. Morley, M. I. Arshad, H.T. Ali, M. Yusuf, Z. Latif, Lanthanum doped $Zn_{0.5}Co_{0.5}La_xFe_{2-x}O_4$ spinel ferrites synthesized via co-precipitation route to evaluate structural, vibrational, electrical, optical, dielectric, and thermoelectric properties, J. Phys. Chem. Solid 154 (2021) 110080.

[22] A.U. Rehman, N. Morley, N. Amin, M.I. Arshad, M.A. un Nabi, K. Mahmood, A. Ali, A. Aslam, A. Bibi, M.Z. Iqbal, Controllable synthesis of La^{3+} doped $Zn_{0.5}Co_{0.25}Cu_{0.25}Fe_{2-x}La_xO_4$ (x= 0.0, 0.0125, 0.025, 0.0375, 0.05) nano-ferrites by sol-gel auto-combustion route, Ceram. Int., 46 (2020) 29297–29308.

[23] M.I. Arshad, M. Hasan, A.U. Rehman, M. Akhtar, N. Amin, K. Mahmood, A. Ali, T. Trakoolwilaiwan, N.T.K. Thanh, Structural, optical, electrical, dielectric, molecular vibrational and magnetic properties of La3+ doped Mg–Cd–Cu ferrites prepared by Co-precipitation technique, Ceram. Int. 48 (2022) 14246–14260.

[24] B. Saravanakumar, R. Mohan, S.-J. Kim, Facile synthesis of graphene/ZnO nanocomposites by low temperature hydrothermal method, Mater. Res. Bull. 48 (2013) 878–883.

[25] J. Zhang, Z. Chen, J. Zhao, Z. Jiang, Microstructure and mechanical properties of aluminium-graphene composite powders produced by mechanical milling, Mech. Adv. Mater. Modern Process. 4 (2018) 1–9.

[26] P. Liu, Y. Huang, X. Zhang, Synthesis and excellent microwave absorption properties of graphene/polypyrrole composites with Fe_3O_4 particles prepared via a co-precipitation method, Mater. Lett. 129 (2014) 35–38.

[27] M. Rahimi-Nasrabadi, M. Rostami, F. Ahmadi, A.F. Shojaie, M.D. Rafiee, Synthesis and characterization of $ZnFe_{2-x}Yb_xO_4$–graphene nanocomposites by sol–gel method, J. Mater. Sci. Mater. Electron. 27 (2016) 11940–11945.

[28] Z. Latifa, A. Rehmana, M. Yusufb, N. Amina, M. Arshada, Estimation of the spectral, electrical, and dielectric properties of Mn-Cu-Cd-Gd ferrite\graphene nanoplatelets composites, J. Ovonic Res. 18 (2022) 627–635.

[29] K. Mehmood, A.U. Rehman, N. Amin, N. Morley, M.I. Arshad, Graphene nanoplatelets/Ni-Co-Nd spinel ferrite composites with improving dielectric properties, J. Alloy. Compd. 930 (2023) 167335.

[30] M. Akram, S. Akhlaq, M.I. Arshad, N. Amin, A.A. Ifseisi, M. Akhtar, N.T.K. Thanh, N. Morley, S. Sadiq, S. Hussain, Improving the structural and transport properties of cadmium ferrites with the addition of cerium for high frequency applications, Solid State Commun. 373 (2023) 115317.

[31] B. Wei, L. Wang, Q. Miao, Y. Yuan, P. Dong, R. Vajtai, W. Fei, Fabrication of manganese oxide/three-dimensional reduced graphene oxide composites as the supercapacitors by a reverse microemulsion method, Carbon 85 (2015) 249–260.

[32] T. Aissou, N. Braidy, J. Veilleux, A new one-step deposition approach of graphene nanoflakes coating using a radio frequency plasma: synthesis, characterization and tribological behaviour, Tribol. Int. 167 (2022) 107406.

[33] A. Aslam, A.U. Rehman, N. Amin, M. Amman, M. Akhtar, N. Morley, M.S. Al-Sharif, M. Hessien, K.A. El-Nagdy, M.I. Arshad, To study the structural, electrical, and magnetic properties of M (M= Mg2+, Mn2+, and Cd2+) doped Cu-Ni-Co-La spinel ferrites, Mater. Chem. Phys. 294 (2023) 127034.

[34] A.U. Rehman, G. Abbas, B. Ayoub, N. Amin, M.A. un Nabi, N.A. Morley, M. Akhtar, M.I. Arshad, M.U. Khalid, M. Afzaal, Impact of Ni2+ on the structural, optical, electrical, and dielectric properties of Cu0.25Co0.25Mg0.5-xNixCe0.03Fe1.97O4 spinel ferrites synthesized via sol-gel auto combustion (SGAC) route, Mater. Sci. Eng. B 291 (2023) 116407.

[35] A. Aslam, A. Razzaq, S. Naz, N. Amin, M.I. Arshad, M.A.U. Nabi, A. Nawaz, K. Mahmood, A. Bibi, F. Iqbal, Impact of lanthanum-doping on the physical and electrical properties of cobalt ferrites, J. Supercond. Nov. Magn. (2021) 1–10.

[36] N. Amin, A. Razaq, A.U. Rehman, K. Hussain, M.A.U. Nabi, N. Morley, M. Amami, A. Bibi, M.I. Arshad, K. Mahmood, Transport Properties of Ce-Doped Cd Ferrites $CdFe_{2-x}Ce_xO$ 4, J. Supercond. Nov. Magn. 34 (2021) 2945–2955.

[37] A. Aslam, A.U. Rehman, N. Amin, M. Amami, M.A.u. Nabi, H. Alrobei, M. Asghar, N. Morley, M. Akhtar, M.I. Arshad, Sol-Gel auto-combustion preparation of M2+= Mg2+, Mn2+, Cd2+ substituted M0.25Ni0.15Cu0.25Co0.35Fe2O4 ferrites and their characterizations, J. Supercond. Nov. Magn. (2022) 1–11.

[38] F. Alresheedi, Structure and spectroscopic ellipsometry studies of nanocrystalline Dy_2O_3 thin films deposited on Al_2O_3 wafers by electron beam evaporation technique, J. Mater. Res. Technol. 12 (2021) 2104–2113.

[39] M. Saravanan, T.S. Girisun, S.V. Rao, Super-paramagnetic and unusual nonlinear absorption switching behavior of an in situ decorated $CdFe_2O_{4-x}$GO nanocomposite, J. Mater. Chem. C 5 (2017) 9929–9942.

[40] M. Khani, G. Ebrahimi, H. Ezatpour, Accumulative extrusion bonding of Mg-Mn-Ca/FA+ GNP hybrid biocomposite: On microstructure evaluation, mechanical and corrosion properties, Mater. Today Commun. 33 (2022) 104426.

[41] Z.Ž. Lazarević, Č. Jovalekić, V.N. Ivanovski, A. Rečnik, A. Milutinović, B. Cekić, N.Ž. Romčević, Characterization of partially inverse spinel $ZnFe_2O_4$ with high saturation magnetization synthesized via soft mechanochemically assisted route, J. Phys. Chem. Solid 75 (2014) 869–877.

[42] N. Parvin, V. Kumar, S.-S. Park, T.K. Mandal, S.W. Joo, Enhanced piezoelectric energy harvesting using hybrid composites of MWCNTs and partially-reduced GO in RTV-SR for stable voltage generation, Surf. Interfaces 44 (2024) 103681.

[43] F.H. Wee, P.J. Soh, A. Suhaizal, H. Nornikman, A. Ezanuddin, Free space measurement technique on dielectric properties of agricultural residues at microwave frequencies, in: 2009 SBMO/IEEE MTT-S International Microwave and Optoelectronics Conference (IMOC), IEEE, 2009, pp. 183-187.

[44] G. Abbas, A.U. Rehman, W. Gull, M. Afzaal, N. Amin, L. Ben Farhat, M. Amami, N. A. Morley, M. Akhtar, M.I. Arshad, Impact of Co2+ on the spectral, optoelectrical, and dielectric properties of Mg0.25Ni0.25Cu0.5−xCoxFe1.97La0.03O4 ferrites prepared via sol–gel auto-combustion route, J. Sol-Gel Sci. Technol. 101 (2022) 428–442.

[45] A.U. Rehman, S. Sharif, H. Hegazy, N. Morley, N. Amin, M. Akhtar, M.I. Arshad, Z. Farooq, Z. Munir, T. Munir, Low dielectric loss, and enhanced magneto-dielectric properties of Cu0.5Cd0.5-xCoxFe2O4 ferrites via Co2+ substitution, Mater. Today Commun. (2023) 105371.

[46] N. Singh, A. Agarwal, S. Sanghi, Dielectric relaxation, conductivity behavior and magnetic properties of Mg substituted Zn–Li ferrites, Curr. Appl. Phys. 11 (2011) 783–789.

[47] Z. Liu, Z. Peng, C. Lv, X. Fu, Doping effect of Sm3+ on magnetic and dielectric properties of Ni-Zn ferrites, Ceram. Int. 43 (2017) 1449–1454.

[48] A.U. Rehman, N. Amin, M.B. Tahir, M.A. un Nabi, N. Morley, M. Alzaid, M. Amami, M. Akhtar, M.I. Arshad, Evaluation of spectral, optoelectrical, dielectric, magnetic, and morphological properties of RE3+ (La3+, and Ce3+) and Co2+ co-doped Zn0.75Cu0.25Fe2O4 ferrites, Mater. Chem. Phys. 275 (2022) 125301.

[49] S. Ikram, J. Jacob, M.I. Arshad, K. Mahmood, A. Ali, N. Sabir, N. Amin, S. Hussain, Tailoring the structural, magnetic and dielectric properties of Ni-Zn-$CdFe_2O_4$ spinel ferrites by the substitution of lanthanum ions, Ceram. Int. 45 (2019) 3563–3569.

[50] M. Sharif, J. Jacob, M. Javed, A. Manzoor, K. Mahmood, M.A. Khan, Impact of Co and Mn substitution on structural and dielectric properties of lithium soft ferrites, Phys. B Condens. Matter 567 (2019) 45–50.

[51] K.L. Routray, S. Saha, D. Behera, Nanosized $CoFe_2O_4$-graphene nanoplatelets with massive dielectric enhancement for high frequency device application, Mater. Sci. Eng. B 257 (2020) 114548.

[52] S. Haque, S.C. Mazumdar, M.N.I. Khan, M.K. Das, Impact of Cr substitution on structural, magnetic, electric and impedance study of Mn-Ni-Zn ferrites, Mater. Sci. Appl. 12 (2021) 121–138.

[53] N. Kumari, V. Kumar, S. Singh, Structural, dielectric and magnetic investigations on Al 3+ substituted Zn-ferrospinels, RSC Adv. 5 (2015) 37925–37934.

[54] Y.T. Ng, W. Kong, K.Y. Tshai, Ni-Zn Ferrite-graphene Nanohybrids: Synthesis and Characterization of Magnetic and Microwave Absorbing Properties, in: MATEC Web of Conferences, EDP Sciences, 2017, pp. 01007.

[55] N.N. Sarkar, K.G. Rewatkar, V.M. Nanoti, N.T. Tayade, Structural, Magnetic-Electrical Behavior of Zr substituted Ni-Zn Spinel Ferrite, Res. J. Sci. Technol. 10 (2018) 13–18.

[56] M.N. Akhtar, M.S. Nazir, M.A. Khan, S. Ullah, M.A. Assiri, Preparations and characterizations of Ca doped Ni–Mg–Mn nanocrystalline ferrites for switching field high-frequency applications, Ceram. Int. 48 (2022) 3833–3840.